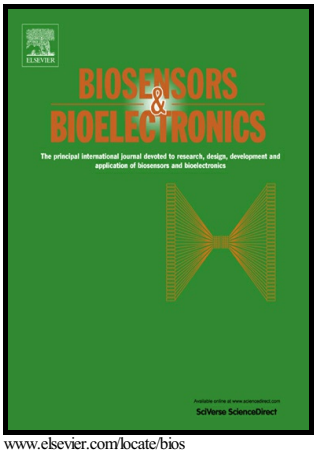

www.elsevier.com/locate/bios

Ultra-high sensitivity of the non-immunological affinity of graphene oxide-peptide-based surface plasmon resonance biosensors to detect human chorionic gonadotropin

Nan-Fu Chiu, Chia-Tzu Kuo, Ting-Li Lin, Chia-Chen Chang, Chen-Yu Chen

PII: S0956-5663(17)30162-8
DOI: http://dx.doi.org/10.1016/j.bios.2017.03.008
Reference: BIOS9596

To appear in: *Biosensors and Bioelectronic*

Received date: 16 December 2016
Revised date: 24 February 2017
Accepted date: 6 March 2017

Cite this article as: Nan-Fu Chiu, Chia-Tzu Kuo, Ting-Li Lin, Chia-Chen Chang and Chen-Yu Chen, Ultra-high sensitivity of the non-immunological affinity of graphene oxide-peptide-based surface plasmon resonance biosensors to detect human chorionic gonadotropin, *Biosensors and Bioelectronic* http://dx.doi.org/10.1016/j.bios.2017.03.008

Ultra-high sensitivity of the non-immunological affinity of graphene oxide-peptide-based surface plasmon resonance biosensors to detect human chorionic gonadotropin

Nan-Fu Chiu[1*], Chia-Tzu Kuo[1], Ting-Li Lin[1], Chia-Chen Chang[2], Chen-Yu Chen[3,4**]

[1]Institute of Electro-Optical Science and Technology, National Taiwan Normal University, No. 88, Sec. 4, Ting-Chou Road, Taipei 11677, Taiwan

[2]Institute of Biomedical Engineering, National Taiwan University, Taipei 10617, Taiwan

[3]Department of Obstetrics and Gynecology, Mackay Memorial Hospital, Taipei 10449, Taiwan

[4]Department of Medicine, Mackay Medical College, Taipei 252, Taiwan

nfchiu@ntnu.edu.tw

f122481@mmh.org.tw

[*]**Correspondence to:** No. 88, Sec. 4, Ting-Chou Road, Taipei 11677, Taiwan**.** Tel.: +886 77346722; fax:+886 2 86631954.

[**]**Corresponding author at:** Department of Obstetrics and Gynecology, Mackay Memorial Hospital, No. 92, Sec. 2, Zhongshan N. Rd., Taipei 10449, Taiwan**.** Tel: +886 2 25433535; fax: +886 2 25433642.

Abstract

Specific peptide aptamers can be used in place of expensive antibody proteins, and they are gaining increasing importance as sensing probes due to their potential in the development of non-immunological assays with high sensitivity, affinity and specificity for human chorionic gonadotropin (hCG) protein. We combined graphene oxide (GO) sheets with a specific peptide aptamer to create a novel, simple and label-free tool to detect abnormalities at an early stage of pregnancy, a GO-peptide-based surface plasmon resonance (SPR) biosensor. This is the first binding interface experiment to successfully demonstrate binding specificity in kinetic analysis biomechanics in peptide aptamers and GO sheets. In addition to the improved affinity offered by the high compatibility with the target hCG protein, the major advantage of GO-peptide-based

SPR sensors was their reduced nonspecific adsorption and enhanced sensitivity. The calculation of total electric field intensity (ΔE) in the GO-based sensing interfaces was significantly enhanced by up to 1.2 times that of a conventional SPR chip. The GO-peptide-based chip (1 mM) had a high affinity (K_A) of 6.37×10^{12} M^{-1}, limit of detection of 0.065 nM and ultra-high sensitivity of 16 times that of a conventional SPR chip. The sensitivity of the slope ratio of the low concentration hCG protein assay in linear regression analysis was GO-peptide (1 mM): GO-peptide (0.1 mM): conventional chip (8-mercaptooctanoic acid)-peptide (0.1 mM)) = 8.6: 3.3: 1. In summary, the excellent binding affinity, low detection limit, high sensitivity, good stability and specificity suggest the potential of this GO-peptide-based SPR chip detection method in clinical application. The development of real-time whole blood analytic and diagnostic tools to detect abnormalities at an early stage of pregnancy is a promising technique for future clinical application.

Keywords

Peptide aptamer, human chorionic gonadotropin (hCG), graphene oxide (GO), surface plasmon resonance (SPR)

1. Introduction

Graphene oxide (GO) can take the form of two-dimensional carbon sheets with various oxygen-containing functional groups on the basal planes and peripheries. It can easily be fabricated on a large scale by using a covalent approach to functionalize nanocomposite materials (Imani et al., 2015; Chiu et al., 2017). GO sheets have many potential applications, and their characteristics have been widely studied. In addition, GO sheets can be controlled by the amount of oxygen-containing functional groups to modulate the characteristics of plasmonic resonance (Angelo et al., 2015; Tararan et al., 2016).

We previously demonstrated the first surface plasmon resonance (SPR) biosensor incorporating GO, and showed the potential of the specific affinity properties of GO in SPR-enhanced biosensing (Chiu et al., 2012; Chiu and Huang, 2014; Chiu et al., 2014). In recent years, GO sheets have been widely used in controllable drug-release carriers to study the characteristics of biomolecular interactions (Sun et al., 2008; Chung et al., 2013; Han et al., 2016), and in immune diagnostic chips (Chiu et al., 2012; Zhang et al., 2013; Chiu et al., 2014; Stebunov et al., 2015; Chiu et al., 2017). The specific hydrophilic affinity, electrostatic, hydrogen-bonding and π-π stacking interactions of GO sheets affect the adsorption capacity of biological molecule immobilization. The many oxygen-containing functional groups on GO sheets can also improve the interface quality of the sensor layer to immobilize biomolecules through covalent binding (Dreyer et al., 2010; Liu et al., 2010; Chung et al., 2013; Chiu and Huang, 2014), which can then control the band gap (Johari and Shenoy, 2011; Bao and Loh, 2012; Shen et al., 2013). Recent studies have reported the use of peptide-based GO sheets in targeted cancer cell therapy (Wang et al., 2014; Wu et al., 2015; Hong et al., 2016) and sensor (Gao et al., 2015; Lim et al., 2015) applications. In these studies, an increasing number of resolved peptide-GO sheet structures have highlighted the interactive mechanisms of the binding interface, and shown that using GO sheets to develop rapid tools to identify important biomarkers in non-immunological diagnostic techniques for diseases in early pregnancy and cancer is a promising technology. Developing a peptide-aptamer-based GO SPR biochip for this purpose, with a label-free mechanism and without requiring expensive antibodies to detect human chorionic gonadotropin (hCG) would be beneficial. Related technologies have successfully used an hCG-binding peptide aptamer in a liquid crystal-based assay (Ding and Yang, 2013) and gold nanoparticle-based colorimetric detection (Chang et al., 2014). However,

this technology has not yet been used in the development of rapid diagnostic biosensors or kinetic analysis for GO-based SPR techniques.

In this study, we investigated the use of a GO-peptide-based SPR chip to enhance the sensitivity of a pregnancy disease assay using hCG protein. We investigated the use of a modified peptide aptamer that can be covalently attached to the surface of GO sheets, and also an enhanced target of the hCG protein assay with GO-peptide specific interactions. In addition, we explored the interaction functions and different response surfaces of the peptide aptamer with GO sheets, and the crucial role of the peptide aptamer binding-site specificity and affinity properties in label-free protein detection. The presence of the hCG protein has been associated with the risk of miscarriage, symptoms of ectopic pregnancy, and some cancerous tumors. Therefore, elevated levels of hCG in patients who are not pregnant can be used to aid in the diagnosis of cancer. This suggests that the development of a GO-peptide-based biosensor with high sensitivity and the ability to rapidly detect the amount of hCG protein would be of clinical value.

2. Materials and Methods

2-1. Preparation of the GO sheets and sensing chip process

We designed optimal experimental conditions to prepare the GO-peptide-based biosensing material. The excellent sensing properties of GO sheets dispersed in water is due to a single atomic layer ratio of more than 80%, and a composition containing functional groups of carbon (79%) and oxygen (20%). The GO sheets were synthesized using a modification of Hummer's method as previously described (Chiu and Huang, 2014).

We fabricated the sensing chip using high performance BK7 substrate, with a 2-nm

chromium (Cr) adhesion layer and a 47-nm gold (Au) film deposited on the BK7 substrate using an electron beam evaporator (Chiu and Huang, 2014) as shown in Figure 1(a). The Au film was chemically modified by derivatization with a thiol self-assembled monolayer (SAM) of cystamine (Cys) (cystamine dihydrochloride 98%, Alfa Aesar) by immersing an electrode in a double-distilled water (ddH2O) solution of Cys (10 mM) for 24 hours at room temperature. Cys is an essential amino acid that contains amine ($–NH_2$) groups on one side and thiol (–SH) groups on the other side as shown in Figure 1(b). Therefore, the Au film had an amine-terminated surface. The Au film was then thoroughly rinsed with ethanol and dried with pure N_2. To immobilize the GO sheets, the Au film was immersed into GO aqueous solution (0.275 and 1 mg/ml). Exposed Cys attached to the Au film could couple with amine (–NH2) groups and covalently couple with carboxyl (–COOH) groups on the GO sheet surfaces. Covalent coupling offers a stable and easy method for bonding surface functionalization on GO sheets. The GO sheets were thoroughly rinsed with deionized water to remove unbonded GO at the Au-link surfaces. The process of fabricating the GO sheets with the Au film is shown in Figure 1(c). The reaction was activated using 10 mg of 1-ethyl-3-(3-dimethylaminopropyl)carbodiimide (EDC) powder in 130 µL of ddH_2O at a concentration of 0.4 M, and 10 mg of N-hydroxysuccinimide (NHS) powder in 865 µl of ddH_2O at a concentration of 0.1 M. The carboxyl end groups on the surfaces of the GO sheets were activated for covalent bond formation to immobilize hydrocarbon chains using 100 µl 0.1 M NHS and 100 µl 0.4 M EDC solutions mixed together. An activation buffer of 200 µl was injected at a flow rate of 60 µl/min in a micro-flow channel system as shown in Figure 1(d). The activated GO surfaces underwent strong covalent immobilization via an amine (NH_2)-coupling reaction in a peptide aptamer probe.

2-2. Preparation of the peptide GO sheet sensing layer and affinity binding reactions

To develop a peptide aptamer probe for short oligopeptide sequences (Ding and Yang, 2013), we used (N-)PPLRINRHILTR(-C) (N-Pro-ProLeu-Arg-Ile-Asn-Arg-His-Ile-Leu-Thr-Arg-C) to assay hCG protein. For the GO sheet bonded peptide aptamer, we used a peptide probe at a concentration of 0.1 mM (or 1 mM) and volume of 200 µl injected at a flow rate of 60 µl/min in a micro-flow channel system to immobilize peptide bonds (amide bonds) on carboxyl bonds on the GO sheet surface using covalent bonds as shown in Figure 1(e). To block potential sites of interaction, the remaining activated carboxyl groups on the GO sheet surfaces were blocked by injecting a very high concentration ethanolamine solution (1 M). The ethanolamine solution was reacted in a 200-µl micro-flow channel system, and a flow rate of 60 µl/min also helped to elute any non-covalently bound material as shown in Figure 1(f). We used 10x phosphate-buffered saline (PBS) solution to dilute a 1x PBS running buffer and to wash non-specific adsorbent proteins from the peptide probe to quantitatively evaluate the label-free specific reactant and affinity separation to identify the number and baseline levels of the detection target hCG proteins as shown in Figure 1(g). The sensing surface could be regenerated with 50 mM sodium hydroxide (NaOH) solution adjusted to pH 2.0. The interaction kinetics of hCG with the biosensors formed by the GO-peptide-based sheets were studied by measuring separate association (k_a) and dissociation (k_d) rate constants in SPR angle changes after the addition of various concentrations of hCG. The experiments tested hCG proteins in serial dilutions of 1x PBS buffer (pH = 7.2) at different concentrations (250 nM to 0.065 nM). In this assay study, we used dual-channel microfluidics with 200 µl of an injected sample of hCG proteins, and calibrated this via standardized 60 m° with 1% ethanol solution in a SPR BI-3000

system (Biosensing Instrument, Tempe, AZ). EDC, NHS, ethanolamine powder and hCG were purchased from Sigma-Aldrich.

3. Results and Discussion

3-1. Surface analysis and sensing film properties

Figure 2(a) shows scanning electron microscope (SEM) images of the GO sheets on the sensing chip. Changes in the surface densities of the Cys-SAM-coated Au films after the adsorption of the GO sheets were associated with 1 mg/ml concentrations of the GO sheet solution. Figure 2(a) also shows that the GO sheets had a relatively large surface (with an edge less than 1 μm), and that they were ultrathin and stacked or continuous, with the edges of individual sheets having a morphology resembling a thin curtain. Supplementary Figure S1 shows the Fourier transformed infrared (FTIR) spectra of the GO sheet film, and Supplementary Figure S2 presents X-Ray photoelectron spectroscopy (XPS) analysis of the Au/GO chip.

Figure 2(b) shows the Nyquist plots of electrochemical impedance spectroscopy (EIS) of bare Au, Au/Cys, Au/Cys/GO and Au/Cys/GO/peptide chips in the presence of pH 7.0 PBS and equimolar 2 mM $[Fe(CN)_6]^{3-/4-}$. The Nyquist plots of different chips were investigated at a frequency range of 10^{-1} to 10^{5} Hz, initial potential of 0.24 v and 12 points per decade under excitation of a sinusoidal wave of 5 mv amplitude. In EIS, the diameter of a semicircle arc in the high frequency region corresponded to the electron transfer resistance, R_{et}. The bare Au electrode showed almost a straight line with a very small semicircle domain (R_{et} = 55.89 ohm), representing the characteristics of diffusion-facilitated electron-transfer processes on the electrode surface. After the Cys film was immobilized on the bare Au, an increase in R_{et} to 110.6 ohm was observed, indicating that the Cys film hindered electron transfer. For

Au/Cys/GO, the value of R_{et} was 844.2 ohm, implying that the incorporation of GO sheets greatly limited electron transfer. There was further immobilization of the peptide aptamer, and the R_{et} of Au/Cys/GO/peptide increased to 909.73 ohm, which was caused by the hindrance of electron transfer. These results confirmed that the peptide aptamer was immobilized successfully onto the chip.

Figure 2(c) shows the results of cyclic voltammograms for the behavior of electrochemically modified sensing film characterization curves of the four different sensing chips obtained at a potential ranging from -0.2 to 0.6 V and scan rate of 50 $mV \cdot s^{-1}$ in 0.1 M KCl solution that also contained 2 mM $[Fe(CN)_6]^{3-/4-}$. The results showed a pair of well-defined quasi-reversible redox peaks at 0.13 V and 0.25 V representing the bare Au and Au/Cys chips. In contrast, the Au/Cys/GO and Au/Cys/GO/peptide chips did not show any redox waves in the potential range studied. The Au/Cys/GO chip yielded a cyclic voltammetry curve that was less than that of the bare Au and Au/Cys chips, representing the presence of oxygen-containing functional groups on the surface of GO leading to decreased electron transfer capability. The Au/Cys/GO/peptide chip had a significantly increased surface impedance, which was due to the peptide having low conductivity and transfer rates leading to transport of the redox species, thereby limiting electron transfer and resulting in the absence of distinct peaks of $[Fe(CN)_6]^{3-/4-}$ and a lower current intensity (Shinwari et al., 2010). The EIS and cyclic voltammogram measurements were made using a CHI model 604D workstation (CH Instruments, Austin, TX, USA).

3-2. Interface analysis of hybrid GO–plasmonic waveguide structures

We designed a series of experimental analyses and theoretical verifications of the GO film

interface in an electric field and its optical properties. The fabrication parameters of the ATR Kretschmann-configuration SPR chips were calculated using Fresnel's equations for a multilayer reflection modeling theory (Lin et al., 2006; Chiu et al., 2014a). The configuration of SPR multilayer layer thicknesses corresponding to the Cr, Au, Cys, and GO films were 2 nm, 47 nm, 0.5 nm and 1.8 nm, respectively. We used the refractive index (*n*) and extinction coefficient (*k*) at a wavelength of 670 nm corresponding to the Cr, Au, Cys, and GO films and obtained 3.717+i4.36, 0.137+i3.56, 1.45+i0 (Rossi et al., 2003), and 1.707+i0.213 (Jung et al., 2008), respectively. Numerical calculations of the SPR curve equation used an excitation wavelength of 670 nm in transverse magnetic (TM) polarization. Different films on the SPR reflectivity curve were measured and fit at incident angles of 30°-42° of the SPR dip (Figure 3(a)). Accordingly, the external angle (θ_{ext}) of incidence was deferent from the internal angle (θ_{int}) within the triangle prism. For clarity, we converted all calculation resonance angles to the external angle (θ_{ext}), and the refraction and possible loss of light at the prism boundaries were disregarded. Roughness crucially affects reflection, scattering and the SPR dispersion relation of light, thereby potentially reducing coupling with the SPR curve (Kanso et al., 2007). Therefore, surface roughness factors caused differences in the calculation and experimental measurements. The theoretical calculation parameters only included the thickness and refractive index of the thin film layer of the material and not roughness on Au, linker, and GO films. Therefore, we used data for the ideal thin film from the theoretical calculations. The measured resonance angles of the SPR reflectivity curve for the Au film, Au-Cys and Au-Cys-GO chips were 33.2°, 33.35° and 33.6°, respectively. The resonance angles for the Au film and Au-Cys chips were 33.2° (43.74°) and 33.35° (43.79°), respectively. For the Au-Cys-GO chips, the resonance angles were 33.51° (43.95°) for a 1.2-nm GO monolayer and 33.6° (44.04°) for a 1.8-mm GO multilayer. These results suggested a GO

concentration of 1 mg/ml at a film thickness of about 1.8 nm.

We then determined the surface plasmon polariton (SPP) oscillation propagation coefficients in the planar total field energy (ΔE) obtained in longitudinal electric fields on layer by layer interfaces (Pitarke et al., 2007; Chiu et al., 2014a).

The effects calculations of different incident angles on the interface electric field of the Au-Cys-GO chip are shown in Figure 3(b). The electric field profiles were calculated at an interior angle of 44.04° and external angle of 33.45°. The longitudinal electric fields in SP energy propagation depended on the dielectric load of the GO films. The local E-field distribution along the stack layer was calculated at the SPR resonance dip. The results showed that the incident light at the same SPR resonance angle had a maximum electric field and large propagation length at the GO film interface. An enhanced electric field intensity was generated around the Au (47 nm)-Cr (2 nm)-Cys (0.5 nm)-GO (1.8 nm)/air interface due to the SPR effect, and the maximum electric field intensity was 154.19 V/m (compared to 126.95 V/m for a conventional Au chip with Au film). The ratio of the total electric field intensity of the GO-based chip versus the conventional Au chip was 1.2:1. Figure 3(b) inset shows the electric field intensity of the Au-Cys-GO interfaces. Supplementary Figure S3(a) shows the calculated angular reflectance dip in resonance for the excitation of the SPPs at the Au/GO biosensor interfaces. Supplementary Figure S3(b) shows the analysis of reflectance SPR dispersion spectra of the GO film thickness. The high electric field enhancement in the vicinity of the GO interface suggested the potential application of GO-based label-free bio-sensing interactions and small molecules for the development of new drugs.

3-3. Biomolecular interaction analysis using GO-peptide and hCG proteins

We used a special sequence peptide aptamer probe to assay hCG. Figures 4(a)-(c) show the GO-based chip responses to the injected peptide at a volume of 200 µl and flow rate of 60 µl/min, which was about 180 s. We then investigated the effects of different concentrations of hCG at an injected volume of 200 µl and flow rate of 60 µl/min in a channel system for equilibrium (Req) analysis in SPR sensorgrams consisting of an association, steady state and dissociation phase on the GO-peptide-based chips as shown in Figure 4. Figure 4(a) shows the ability of the GO-peptide (0.1 mM) chip and Figure 4(b) shows the ability of the GO-peptide (1 mM) chip to detect different concentrations of hCG protein. The shift in SPR angle at equilibrium (Req) for the GO-peptide (0.1 mM) chip at hCG protein concentrations of 166.6, 100, 33.32, 25 and 8.32 nM were 44.457, 29.415, 13.239, 11.683, and 9.83 m°, respectively. From these results, the equilibrium time was determined to be 250 s. The SPR sensorgram equilibrium angles for the GO-peptide (1 mM) chip at hCG protein concentrations of 250, 166.6, 125, 100, 33.32, 25 and 4.16 nM were 64.595, 64.131, 62.33, 49.752, 32.434, 19.119 and 7.008 m°, respectively. Figure 4(c) shows that the equilibrium analyses were in good agreement with the calibration curve. The linear fitting of the GO-peptide (0.1 mM) and GO-peptide (1 mM) chips showed SPR sensorgram equilibrium for hCG concentrations ranging from 4.16 to 250 nM. When the hCG protein concentrations were higher than 125 nM on the GO-peptide (1 mM) chip, the SPR shift angle gradually approached a steady state for saturation. We performed linear regression analysis before reaching saturation. The linear regression equation was $y = 6.65 + 0.23x$ with a correlation coefficient (R^2) of 0.995 for the GO-peptide (0.1 mM) chip, and $y = 10.05 + 0.42x$ and a R2 of 0.933 for the GO-peptide (1 mM) chip, where y represents the SPR angle (m^o), and x

is the hCG concentration.

Supplementary Figure S4 shows the self-assembly and interface properties of the GO-based and the conventional Au based SPR sensing films. Supplementary Figures S4(a)-S4(c) show real-time sensorgrams with all steps of Cys coupling, deactivation, GO-peptide binding, and regeneration, and Supplementary Figure S4(d) shows that the affinity binding constant (K_A) of the GO film to the peptide aptamer was increased by up to 5.24 times. Supplementary Figures S4(e) and S4(f) show that the binding efficiency of the dissociation constant (K_D) for the conventional chip with respect to the peptide aptamer was 7.25 times higher than that of the GO-based chip. This suggests that GO-based chips are more suitable for affinity binding to a peptide aptamer.

3-4. Ultrasensitive detection for affinity and kinetics analysis of binding interactions

We next investigated the increase in peptide aptamer probe concentration on the GO films, and increased the immobilization time to enhance the detection sensitivity. Figures 5(a)-(d) show the bonding peptide aptamer immobilization on the GO films stored in a refrigerator at 4^{o}C for 4 hours. A series of low concentrations of hCG protein were reacted in a 200-µL micro-flow channel system at a flow rate of 60 µL/min. The SPR-chip was then gently dissociated and the sensing surface was regenerated with 50 mM NaOH at a flow rate of 60 µL/min. Figures 5(a), 5(b) and 5(c) show that the MOA (1 mM)-peptide (0.1 mM), GO-peptide (0.1 mM) and GO-peptide (1 mM) chips in SPR sensorgrams in equilibrium analysis could detect low hCG concentrations ranging from 0.065 to 8.32 nM. The SPR sensorgrams were prepared by injecting hCG samples at different concentrations when the SPR angle equilibrium time was set at 250 s. Figure 5(a) shows that for the MOA (1 mM)-peptide (0.1 mM) chip, the SPR sensorgram

equilibrium angles for hCG protein concentrations of 8.32, 4.16, 2.08 and 1.04 nM were 34.551, 11.831, 4.68 and 3.236 m°, respectively. Figure 5(b) shows that for the GO-peptide (0.1 mM) chip, the SPR sensorgram equilibrium angles for hCG protein concentrations of 0.52, 0.39, 0.26, 0.19 and 0.13 nM were 11.385, 9.036, 8.174, 6.575 and 5.271 m°, respectively. Figure 5(c) shows that for the GO-peptide (1 mM) chip, the SPR sensorgram equilibrium angles for hCG protein concentrations of 0.346, 0.281, 0.195, 0.13 and 0.065 nM were 13.706, 11.219, 6.458, 5.382 and 3.045 m°, respectively. The limit of detection (LOD) concentrations for the SPR sensorgram of the MOA (1 mM)-peptide (0.1 mM), GO-peptide (0.1 mM) and GO-peptide (1 mM) chips were 1.04, 0.13 and 0.065 nM, respectively. Comparisons of the hCG protein LOD values between the conventional chip (MOA-peptide (0.1 mM)) and GO-peptide (1 mM) chip and the conventional chip (MOA-peptide (0.1 mM)) and GO-peptide (0.1 mM) chip yielded relative values of 16- and 8-fold.

Figure 5(d) shows the linear regression equations of the calibration curves for the GO-peptide (0.1 mM) and GO-peptide (1 mM) chips: $y = 3.72 + 14.66x$ with a correlation coefficient $R^2 = 0.957$, and $y = 0.12 + 38.95x$ with a correlation coefficient $R^2 = 0.965$, respectively. Figure 5(d) inset shows the linear regression equations of the calibration curves for the conventional chip (MOA-peptide (0.1 mM)): $y = -3.74 + 4.44x$ with a correlation coefficient $R^2 = 0.961$. Comparisons of the experimental results are shown in Figure 5(d), in which an increased peptide aptamer probe immobilization time of 4 hours achieved high detection sensitivity and low detection limit. The linear regression curves of the slope of each fitting curve were: 4.44 for the conventional chip (MOA-peptide (0.1 mM)), 14.66 for the GO-peptide (0.1 mM) chip, and 38.34 for the GO-peptide (1 mM) chip. A large slope represented high sensitivity of the SPR sensor. The results showed that the device with the highest resolution was the

GO-peptide (1 mM) chip. The ratio between the slopes of the linear regression equations of GO-peptide (1 mM): GO-peptide (1 mM): conventional chip (MOA-peptide (0.1 mM)) was 8.6: 3.3: 1. The experimental results showed that the GO-peptide (1 mM) chip had high affinity, ultra-high assay sensitivity and LOD of 0.065 nM. Consecutive injections were reproducible, showing the extent of GO-peptide-based film stability and high affinity of the sensing film surface.

This kinetic analysis is important as it provides dynamic and kinetic parameters. Dissociation was achieved with continuous washing to remove any released hCG protein from the micro-flow channel system. Figure 5(a) shows that due to an excess of non-specific binding, the conventional chip (MOA-peptide (0.1 mM)) did not fit binding interface kinetic analysis. Figures 5(b) and 5(c) show that an excellent fit with kinetic analysis was achieved. In kinetic analysis, the SPR sensorgram appeared to show that the hCG protein molecular binding interfaces for each channel at varying concentrations fit the kinetic analysis (Figs. 5(e) and 5(f)). The typical protein association rate constant (k_a) ranged from 10^3–10^7 $M^{-1}s^{-1}$, and the equilibrium association constant ($K_A = k_a/k_d$) ranged from 10^5–10^{12} M^{-1} (Tudos and Schasfoort, 2008).

The results of the GO-peptide-based chips met the standard average of k_a and K_A. The kinetics of the GO-peptide (1 mM) chip fit the data very closely and yielded a maximum affinity binding constant K_A of 6.37×10^{12} M^{-1} at a concentration of 0.191 nM, and a maximum associated rate constant k_a of 6.0×10^9 $M^{-1}s^{-1}$ at a concentration of 0.281 nM. The kinetics of the GO-peptide (0.1 mM) chip at maximum K_A and k_a were 1.75×10^{12} M^{-1} at a concentration of 0.39 nM and 6.0×10^9 $M^{-1}s^{-1}$ at a concentration of 0.346 nM.

In addition to the improved non-specificity offered by the high affinity binding with the

hCG proteins, the major advantage of the GO-peptide-based chip was in preventing rebinding of protein during the dissociation phase. The ability to simplify an ultrasensitive non-immunosensor was based on the selective and specific interactions between the peptide aptamer and hCG protein for affinity analysis. The GO-peptide-based chips had a high affinity for the hCG assay.

4. Conclusions

We demonstrated that GO-peptide-based chips can provide excellent sensitivity for the early detection of diseases in pregnant women or species that have a high affinity for analyte biomolecules. We also successfully showed that the oxygen-containing functional groups of GO sheets can modulate and enhance plasmonic resonance energy in the visible excitation wavelength range. The concentration of oxygen-rich functional groups of GO should also render it a good biosensing substrate for peptide immobilization through covalent binding. In addition to the highly specific and biostability of the GO film to the peptide aptamer, the significantly increased response affinity binding (K_A) by up to 5.24 times may lead to higher quality biosensing films. The experimental results showed that the GO-peptide-based chip had high sensitivity, high affinity and more specificity and selective interactions between hCG proteins. In addition, the GO-peptide (1 mM) chip had a hCG detection limit 16 times higher than that of a conventional chip (MOA-peptide (0.1 mM)), and a LOD of 0.065 nM. The experimental data had good agreement when fitted to the calibration curve of the GO-peptide-based chip, showing that the linear regression slope was 8.6 times more sensitive with the GO-peptide (1 mM) chip than with the conventional chip (MOA-peptide (0.1 mM)).

The development of peptide aptamers has emerged as a non-immunological method for detection biosensors for the precise and selective measurement of disease proteins in early pregnancy at

low levels, and this may help in the diagnosis of diseases such as Down syndrome, preeclampsia, preterm birth and paraneoplastic syndromes. The excellent affinity, low detection limit, high sensitivity, good stability, and good specificity make GO-peptide-based biosensors a potential candidate for future clinical application.

Acknowledgements

The authors would like to thank the Ministry of Science and Technology of the Republic of China, Taiwan, for financially supporting this research under Contract No. MOST 104-2221-E-003-023, MOST 105-2221-E-003-027 and MOST 104-2314-B-195-015, with Mackay Hospital Project No. MMH-CT-10408 and MMH-CT-10505.

References

Angelo, D. D', Bongiorno, C., Amato, M., Deretzis, I., Magna, A. La, Compagnini, G., Spano`, S.F., Scalese, S., 2015. Electron energy-loss spectra of graphene oxide for the determination of oxygen functionalities. Carbon 93, 1034–1041.

Bao, Q., and Loh, K. P., 2012. Graphene photonics, plasmonics, and broadband optoelectronic devices, ACS nano. 6, 3677-3694.

Chang, C.-C., Chen, C.-P., Lee, C.-H., Chen, C.-Y., and Lin, C.-W., 2014. Colorimetric detection of human chorionic gonadotropin using catalytic gold nanoparticles and a peptide aptamer. Chem. Commun., 50, 14443.

Chiu, N.-F., Huang, T.-Y., Kuo, C.-C., Lee, W.-C., Hsieh, M.-H., Lai, H.-C., 2012. Single-layer graphene based SPR biochips for tuberculosis bacillus detection. Proc. SPIE, 8427,

84273M-7.

Chiu, N.-F., Huang, T.-Y., 2014. Sensitivity and kinetic analysis of graphene oxide-based surface plasmon resonance biosensors. Sens. Actuators. B. 197, 35–42.

Chiu, N.-F., Huang, T.-Y., Lai, H.-C., Liu, K.-C., 2014. Graphene oxide-based SPR biosensor chip for immunoassay applications. Nanoscale Res Lett. 9, 445-451.

Chiu, N.-F., Fan, S.-Y., Yang, C.-D., Huang, T.-Y., 2017. Carboxyl-functionalized graphene oxide composites as SPR biosensors with enhanced sensitivity for immunoaffinity detection. Biosens. Bioelectron., 89, 445–450.

Chiu, N.-F., Tu, Y.-C., Huang, T.-Y., 2014a. Enhanced Sensitivity of Anti-Symmetrically Structured Surface Plasmon Resonance Sensors with Zinc Oxide Intermediate Layers. *Sensors*, *14*, 170-187.

Chung, C., Kim, Y.K., Shin, D., Ryoo, S.R., Hong, B.H., Min, D.H., 2013. Biomedical applications of graphene and graphene oxide, Acc. Chem. Res. 46, 2211–2224.

Ding, X., and Yang, K.-L., 2013. Antibody-free detection of human chorionic gonadotropin by use of liquid crystals. Anal. Chem., 85, 10710−10716.

Dreyer D.R., Park S., Bielawski C.W., Ruoff R.S. 2010. The chemistry of graphene oxide. Chem. Soc. Rev., 39, 228.

Gao, L., Li, Q., Li, R., Yan, L., Zhou, Y., Chen, K., and Shi, H., 2015. Highly sensitive detection for proteins using graphene oxide-aptamer based sensors, Nanoscale, 7, 10903-10907.

Han, U., Seo, Y., and Hong, J., 2016. Effect of pH on the structure and drug release profiles of layer-by-layer assembled films containing polyelectrolyte, micelles, and graphene oxide. Scientific Reports 6, Article number: 24158 .

Hong, E. J., Choi, D. G., Shim, M. S., 2016. Targeted and effective photodynamic therapy for

cancer using functionalized nanomaterials, Acta Pharmaceutica Sinica B, 6(4), 297–307.

Imani, R., Emami, S.H., Faghihi, S., 2015. Synthesis and characterization of an octaarginine functionalized graphene oxide nano-carrier for gene delivery applications. Phys. Chem. Chem. Phys. 17, 6328–6339.

Jung, I., Vaupel, M., Pelton, M., Piner, R., Dikin, D. A., Stankovich, S., An, J., Ruoff, R. S., 2008. Characterization of Thermally Reduced Graphene Oxide by Imaging Ellipsometry. *J. Phys. Chem. C*, 112, 8499–8506.

Johari, P., and Shenoy, V. B., 2011. Modulating optical properties of grapheme oxide: role of prominent functional groups. ACS Nano. 5, 7640-7647.

Kanso, M., Cuenot, S., Louarn, G., 2007. Roughness effect on the SPR measurement for an optical fiber configuration: experimental and numerical approaches. J. Opt. A: Pure Appl. Opt. 9, 586–592.

Lin, C.-W., Chen, K.-P., Su, M.-C., Hsiao, T.-C., Lee, S.-S., Lin, S., Shi, X.-j., Lee, C.-K., 2006. Admittance loci design method for multilayer surface plasmon resonance devices. Sens. Actuators B Chem., 117, 219–229.

Lim, S. K., Chen, P., Lee, F. L., Moochhala, S., and Liedberg, B., 2015. Peptide-Assembled Graphene Oxide as a Fluorescent Turn-On Sensor for Lipopolysaccharide (Endotoxin) Detection, Anal. Chem., 87, 9408−9412.

Liu, Y., Yu, D., Zeng, C., Miao, Z., and Dai, L., 2010. Biocompatible graphene oxide-based glucose biosensors. Langmuir, 26 (9), 6158–6160.

Pitarke, J.M., Silkin, V.M., Chulkov, E.V., Echenique, P.M., 2007. Theory of surface plasmons and surface-plasmon polaritons. Rep. Prog. Phys., 70, 1–87.

Rossi, C., Homand, J., Bauche, C., Hamdi, H., Ladant, D., Chopineau, 2003. Differential

Mechanisms for Calcium-Dependent Protein/Membrane Association as Evidenced from SPR-Binding Studies on Supported Biomimetic Membranes, J. Biochemistry, 42 (51), 15273-15283.

Shen, Y., Yang, S., Zhou, P., Sun, Q., Wang, P., Wan, L., Li, J., Chen, L., Wang, X., Ding, S., Zhang, D. W., 2013. Evolution of the band-gap and optical properties of graphene oxide with controllable reduction level. Carbon, 62, 157–164.

Shinwari, M. W., Deen, M. J., Starikov, E. B., and Cuniberti, G., 2010. Electrical conductance in biological molecules. Adv. Funct. Mater. 20, 1865–1883.

Stebunov, Y.V., Aftenieva, O.A., Arsenin, A.V., Volkov, V.S., 2015. Highly sensitive and selective sensor chips with graphene-oxide linking layer. ACS Appl. Mater. Interfaces 7, 21727–21734.

Sun, X., Liu, Z., Welsher, K., Robinson, J.T., Goodwin, A., Zaric, S., Dai, H., 2008. Nanographene oxide for cellular imaging and drug delivery. Nano Res. 1 (3), 203–212.

Tararan, A., Zobelli, A., Benito, A. M., Maser, W. K., and Stéphan, O., 2016. Revisiting Graphene Oxide Chemistry via Spatially-Resolved Electron Energy Loss Spectroscopy. *Chem. Mater.*, 28 (11), pp 3741–3748.

Tudos, A. J., Schasfoort, R. B. M., 2008. Introduction to Surface Plasmon Resonance. In Handbook of Surface Plasmon Resonance; Schasfoort, R. B. M., Tudos, A. J., Eds.; Royal Society of Chemistry, pp 1-14.

Wang, H., Gu, W., Xiao, N., Ye, L., Xu, Q., 2014. Chlorotoxin-conjugated graphene oxide for

Wu, J., Chen, A., Qin, M., Huang, R., Zhang, G., Xue, B., Wei, J., Li, Y., Cao, Y., and Wang, W., 2015. Hierarchical construction of a mechanically stable peptide–graphene oxide hybrid hydrogel for drug delivery and pulsatile triggered release in vivo, Nanoscale, 7, 1655–1660.

Zhang, H., Sun, Y., Gao, S., Zhang, J., Zhang, H., Song, D., 2013. A novel graphene oxide-based surface plasmon resonance biosensor for immunoassay. Small, 9, 2537–2540.

Figure Captions:

Figure 1. The GO-peptide-based SPR biochip experimental conditions.

Figure 2. (a) Scanning electron microscope micrograph of GO-sensing film. (b) Electrochemical impedance spectroscopy (EIS) characterization of different modified sensing films: bare Au (square); Au/Cys (circle); Au/Cys/GO (triangle); and Au/Cys/GO/Peptide (diamond). (c) Cyclic voltammograms (CVs) of the different sensing chips measured in a 2 mM $[Fe(CN)_6]^{3-/4-}$ solution containing 0.1 M KCl at a scan rate of 50 mV/s.

Figure 3. (a) Theoretical (dashed lines) and measured (solid lines) reflectance SPR curves for different sensing chips at a wavelength of 670 nm tested in an air medium environment. (b) The electric field intensity was highest with maximum coupling of the incident excitation light at a wavelength of 670 nm on GO-based sensing chips.

Figure 4. SPR sensorgrams obtained in response to hCG protein of different concentrations flowing over the surfaces of the sensors. (a) Interaction with the GO-peptide (0.1 mM). (b) interaction with the GO-peptide (1 mM). (c) Equilibrium analysis of binding of the GO-peptide-based chips to a high affinity hCG protein.

Figure 5. (a) Sensorgrams of hCG protein (low concentration: range 8.32~0.065 nM) binding to immobilized GO-peptide with various binding capacities. (a) Conventional chip (MOA-peptide (0.1 mM)). (b) GO-peptide (0.1 mM) chip. (c) GO-peptide (1 mM) chip. (d) Linear regression equations of the calibration curves in SPR equilibrium analysis with binding of hCG protein to a medium-high affinity surface of the GO-peptide chips. Distribution analysis of the interaction of the hCG domain with GO-peptide-based chips. Experimental kinetic binding data fit the analysis of the (e) association (k_a) rates and also determined (f) K_A using the simultaneous k_a/k_d model evaluation of different analyte concentrations. The resulting distribution was very detailed, resolving multiple classes of different concentrations.

Figure 1.

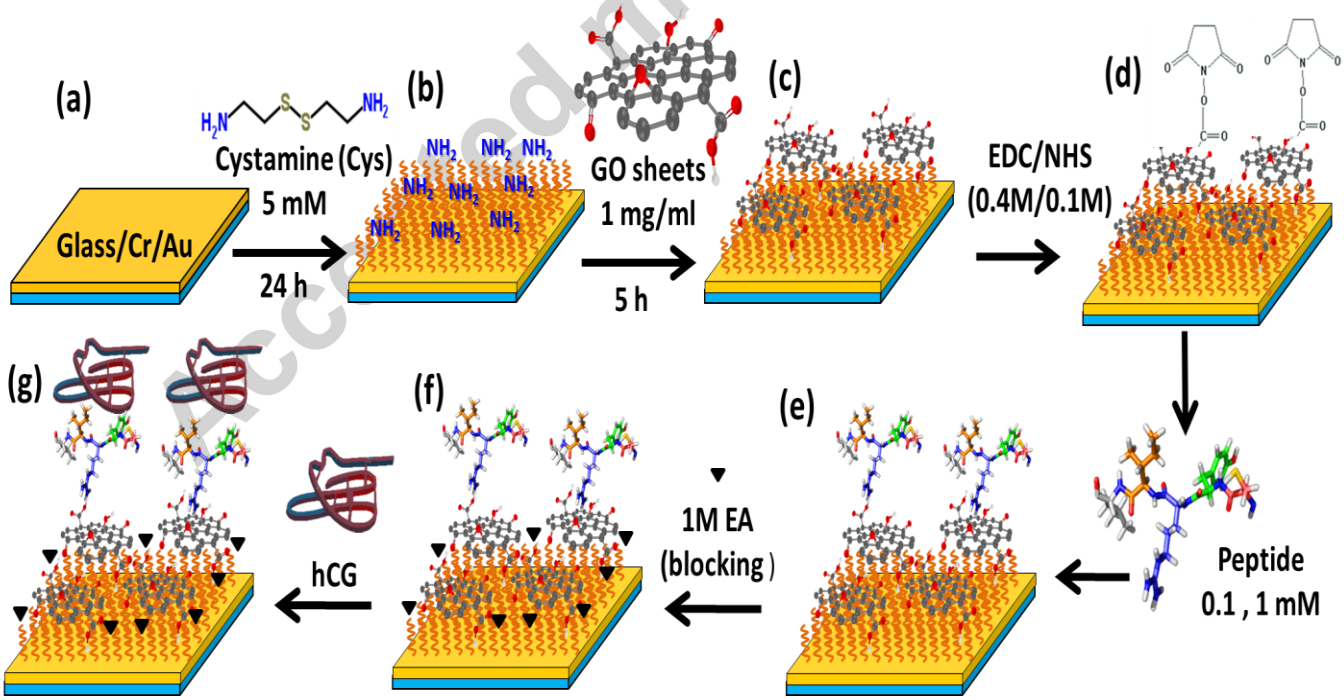

Figure 2.

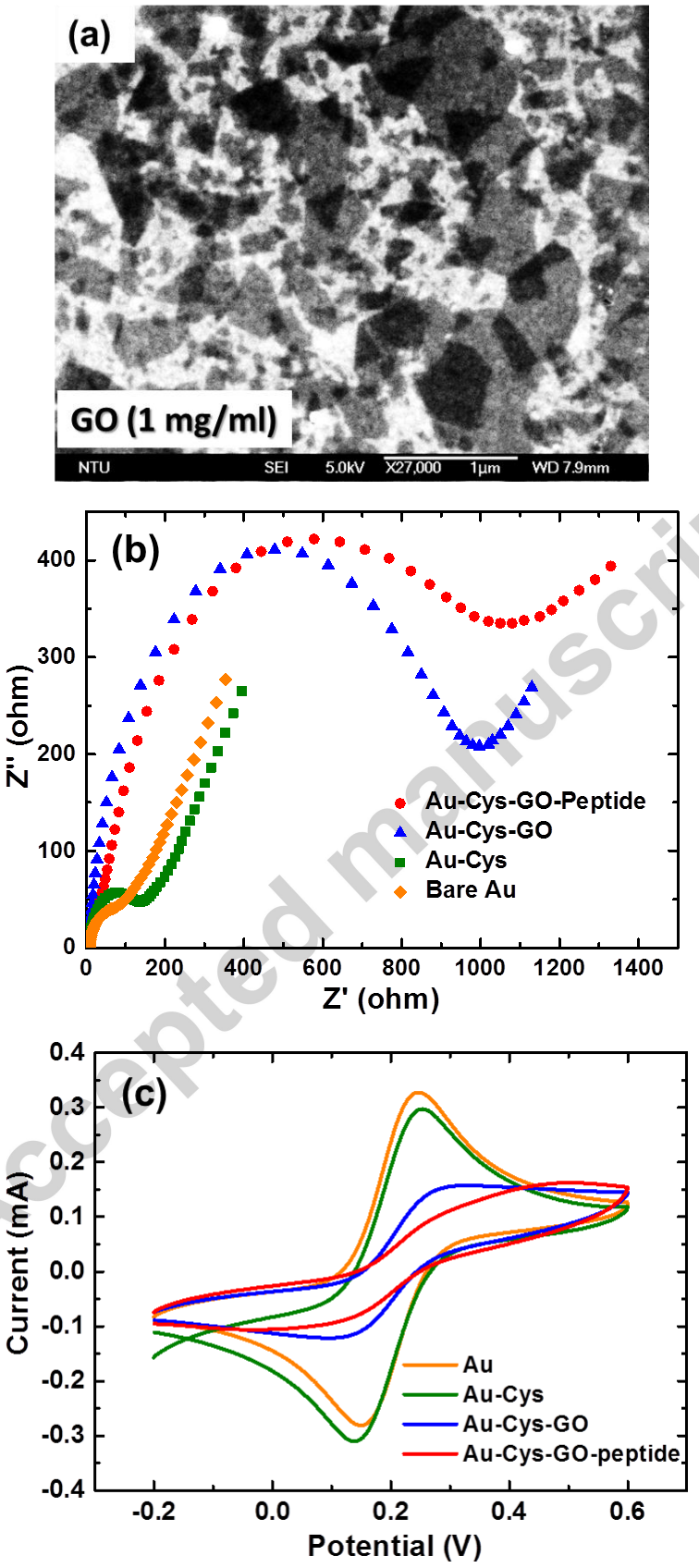

Figure 3.

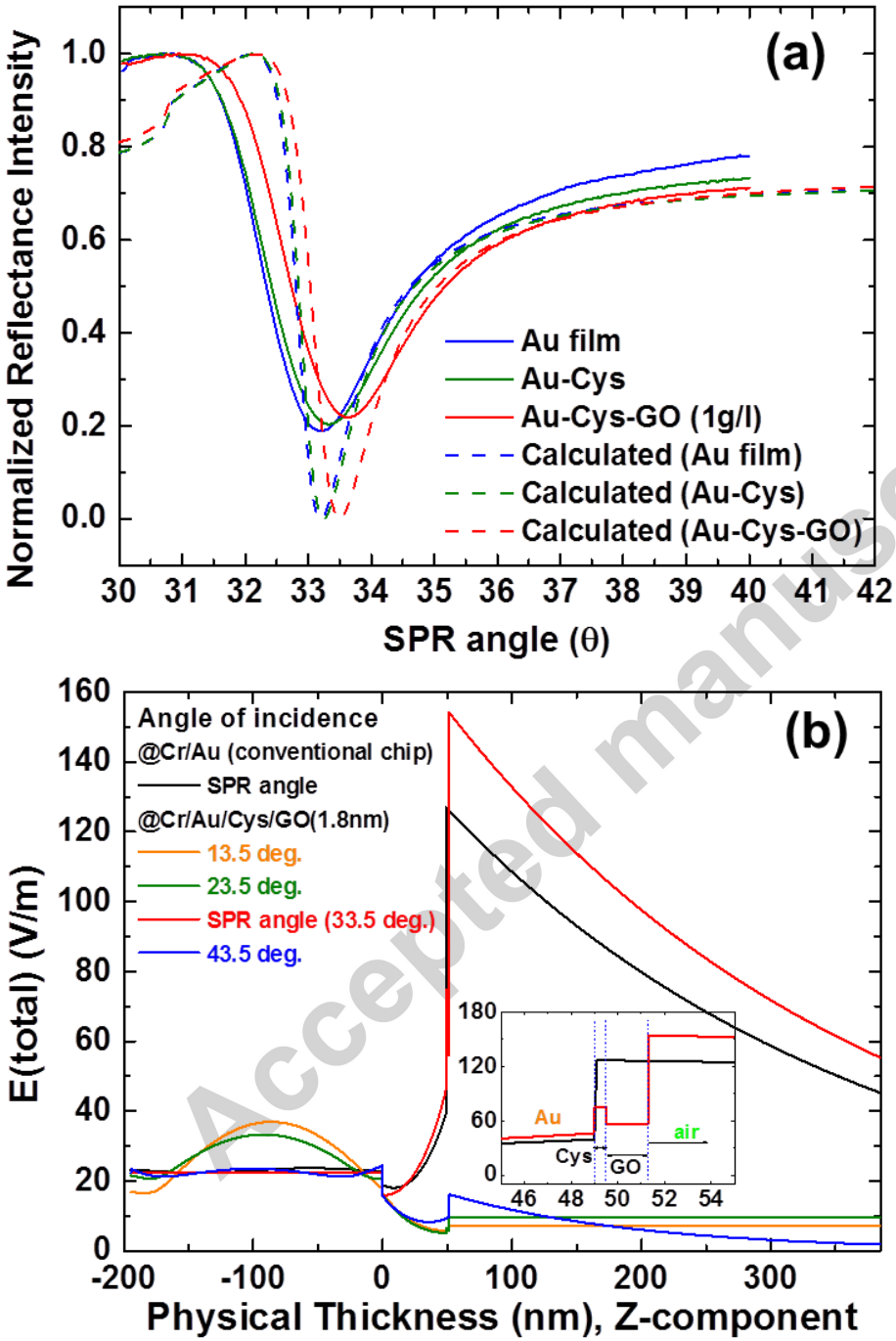

Figure 4.

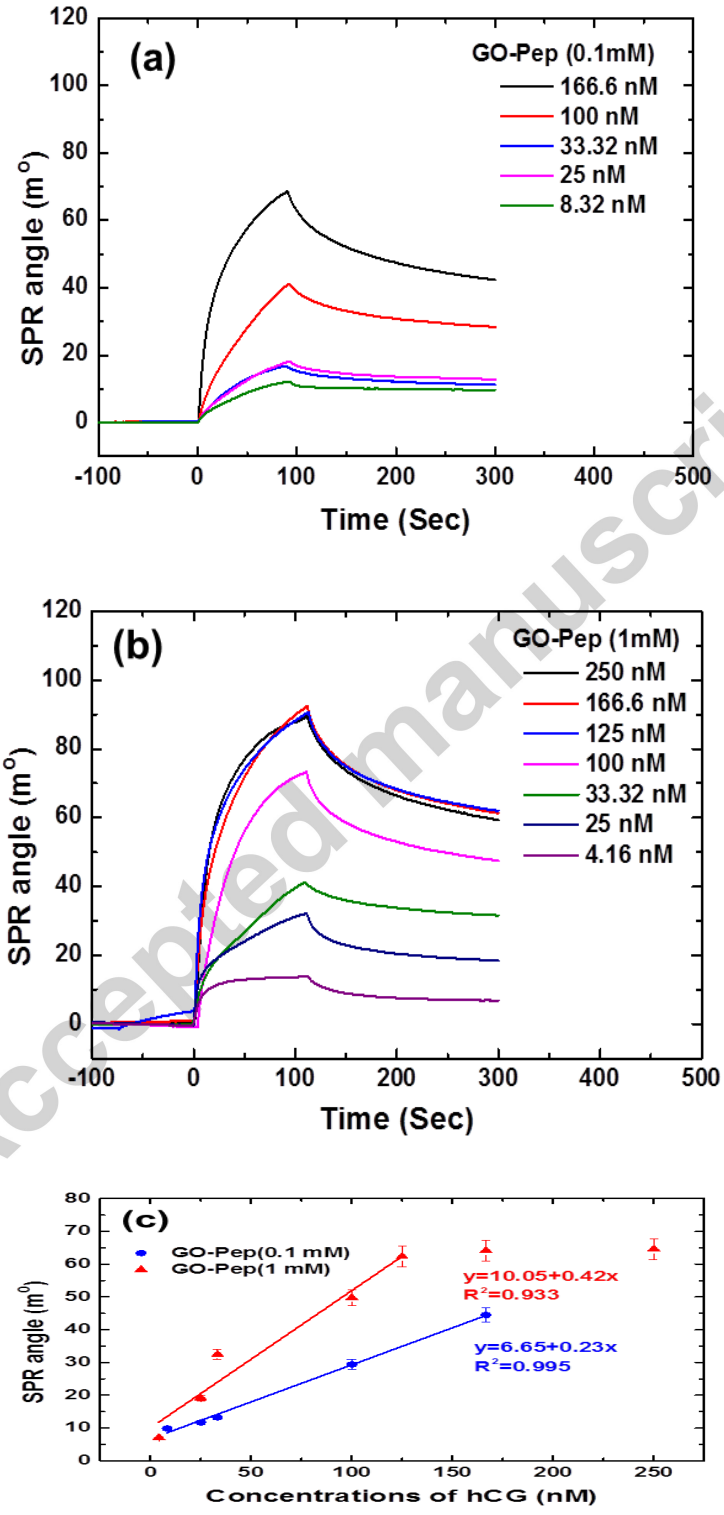

Figure 5.

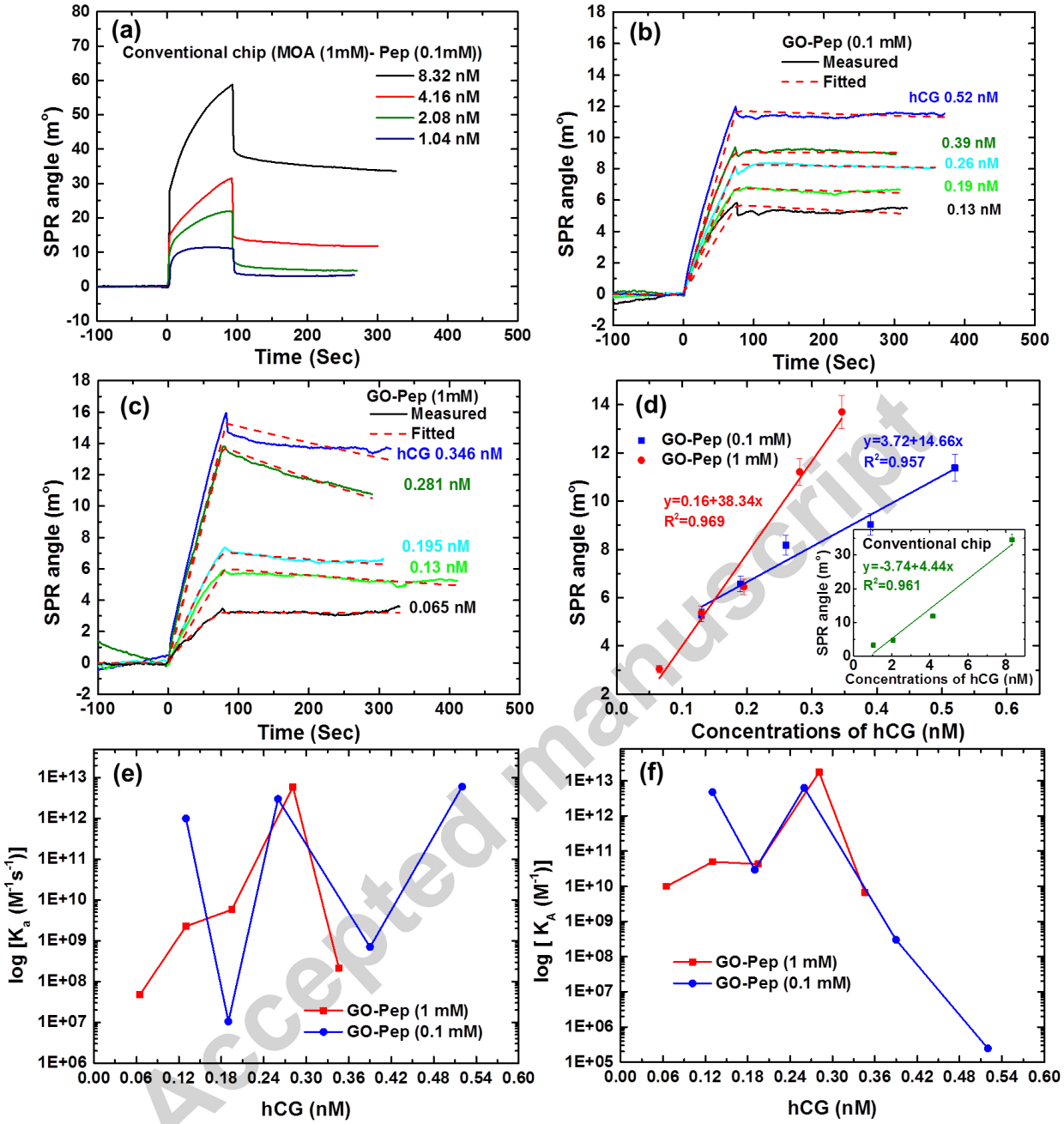

Highlights

- We demonstrate the design of a novel graphene oxide (GO)-peptide-based surface plasmon resonance (SPR) biosensor.
- The GO-peptide-based chip had a high affinity of 6.37×10^{12} M^{-1}, limit of detection of 0.065 nM and ultra-high sensitivity of 16 times that of a conventional SPR chip.
- The high specificity and biostability of the GO film to the peptide aptamer increased affinity binding by up to 5.24 times.
- The sensitivity of the slope ratio of low concentrations of hCG protein in linear regression analysis was GO-peptide: conventional chip = 8.6: 1.